RAMAN MEASUREMENTS OF

DYE-LASER-ANNEALED, ION IMPLANTED GaAs

by

HUADE YAO

Certificate (B.S. Level), Shanghai Normal University, 1983

A MASTER'S THESIS

submitted in partial fulfillment of the

requirements for the degree

MASTER OF SCIENCE

Department of Physics

KANSAS STATE UNIVERSITY

Manhattan, Kansas

1986

Approved by:

Major Professor

TABLE OF CONTENTS

LIST OF FIGURES

LIST OF TABLES

ACKNOWLEDGMENTS

I would like to give my deep thanks to my major professor, Alvin Compaan, for his invaluable guidance, help and support.

I am indebted to professors R.D. Dragsdorf and T. Rahman for serving on my committee.

Thanks are also due to professor C.M. Sorensen for the emergency use of an Ar laser for part of this work.

I would like to express my appreciation to my wife, Linda, for her love and encouragement. A very special thanks also goes to my mother, Enren Xu, for her love, patience and support.

The partial support of the U.S. Office of Naval Research in the early phases of this work is gratefully acknowledged.

Chapter 1

Introduction

Ion Implantation

In semiconductor applications, it is important to be able to introduce impurities into the semiconductor material. The purpose is to produce changes in electrical and optical properties which can make these materials more efficient and suitable for devices. There are mainly two ways to do the doping: diffusion and ion implantation.

Traditionally semiconductor materials are doped by diffusion. There are two steps to achieve this: deposition and diffusion. First, a layer of the dopant is placed on a semiconductor surface. Together they are placed in a high temperature furnace, below the melting point of the materials involved, in an atmosphere of nitrogen or other appropriate gas. In this way the diffusion takes place. In the whole diffusion process several important factors need to be well controlled: dopant concentration, dopant thickness, ambient gas temperature, gas pressure, and diffusion time.

The technology of using high energy ion beams in the keV or MeV range to bombard the solid surface of a semiconductor material to introduce impurities into the crystal is known as ion implantation. Because of its advantages of easy dose control (concentration and depth), spatial masking and low temperature doping, the technique of ion implantation has been widely used to replace the technique of diffusion.

But there are two major problems in processing semiconductors with this technique. One is the damage to the crystalline structure in the near surface region of the material. The ions which have been accelerated by a

high voltage difference are slowed down in the crystalline lattice by displacing a number of lattice atoms. So the lattice structure becomes disordered. The energy needed to displace one lattice atom has been estimated as about is ~25 eV.[1] As an example, a Sn ion with energy of 100 keV would displace ~$4X10^3$ atoms and thus an ion beam like Sn or Cd with energy of the order of keV or MeV at certain dose can cause heavy damage. Our experimental data show that a dose of the order of $10^{15}/cm^2$ for Sn and Cd at ~100 keV causes an amorphous surface layer (~ 30 nm) in GaAs.

The second major problem is that the electrical activation of the implanted dopants is very poor unless subsequent annealing is used in the as-implanted region.

Annealing

In order to remove the surface damage of the crystal and activate the implanted dopants electrically some form of annealing must be used. There are mainly three ways to do the annealing: furnace annealing, rapid thermal annealing (RTA) and laser annealing. Each is described in more detail below.

Furnace annealing: The damaged crystal is put into an oven and heated to ~2/3 of the melting point of the material for 30 minutes or longer.[2] This method is the conventional way to treat implanted semiconductors. However it is often accompanied by undesirable consequences such as decomposition of the crystal surface in the case of compound semiconductors. Furthermore it requires the contacts and the whole crystal to be heated.

Rapid thermal annealing (RTA)[3,4,5]: An implanted semiconductor wafer is heated by radiation of a tungsten-halogen, an arc-lamp, or a graphite heater. A rather uniform temperature is produced throughout the wafer for periods of 1-100 seconds which is much shorter than the furnace annealing

time. RTA is a combination of high temperature (within 100 to 200°C of the melting point) and short time. However, it has problems similar to that mentioned above for furnace annealing.

Laser annealing: A laser beam with appropriate energy density, pulse duration and wavelength is used to heat the surface of the damaged crystal to accomplish annealing.

The laser annealing technique has several advantages. First, the annealing can be done within a desired area simply by focusing the incident laser beam to the desired dimensions. Second, because the laser light is heavily absorbed by the thin surface layer, only the few hundred to a few thousand angstroms of the implanted surface layer which is damaged is heated to a very high temperature and the undamaged substrate is not heated significantly. Third, because the laser annealing speed is extremely fast (~100 nsec), it can be carried out in air.

Because it has advantages over thermal annealing, the laser annealing technique has raised much interest for processing of ion implanted semiconductor materials such as Si and GaAs.[6]

Epitaxial Regrowth

When a damaged part of the crystal is illuminated by a laser beam, the temperature of the near surface region rises rapidly (5-10 nsec) to the melting point and cools off quickly. If the laser beam energy is high enough to melt the surface region down to the undamaged crystalline structure of the substrate, the regrown surface will duplicate the crystalline structure of the substrate. This is known as epitaxial regrowth. By epitaxial regrowth we can remove almost totally the damage caused by ion implantation.

However, when the laser beam energy is not high enough to melt from the surface down to the crystalline substrate, the regrown structure is poly-

crystalline having a grain size which is a function of the laser annealing energy. The orientations of the grains are random.

The surface structure of an ion-implanted GaAs material before and after laser annealing is sketched in Figure 1.

Brief Review of the Literature and the Motivation of Our Study

Pulsed laser annealing (PLA) of GaAs and other III-V semiconductors like GaP and InP have been studied previously but far less than silicon. There is a consensus that PLA of GaAs yields no carrier electrical activation for doses below $10^{14}/cm^2$ range. However, at much higher doses carrier activation may exceed these of furnace annealed samples by at least a factor of ten. Recently, Nojima[7] has made a complete study of this dependence. He considered four factors which might plausibly account for the dose dependence of carrier activation: (1) Cr segregation during PLA; (2) laser irradiation defects produced by the pulsed ruby laser; (3) insufficient laser energy absorption; (4) residual implantation damage. A detailed study denies factors (1)-(3) to be its origin. He found that factor (4) is responsible for the poor carrier activation at low implantation dose. Later, however, Oraby, et al.,[8] found that 1.06 μm pulsed Nd:YAG laser produced much better annealing than a pulsed ruby laser. They attributed this to the low cooling rate produced by IR pulses which penetrate more deeply and are absorbed only in amorphous GaAs.

Therefore, the origin of the poor carrier activation of implants is still unclear. Several questions remain unanswered. What is the pulsed laser annealing threshold for epitaxial regrowth in implanted GaAs and how does the electrical carrier activation depend on laser annealing energy density in case of high doses in GaAs? How does the depletion layer change under different pulsed laser annealing energies? What are the differences

Figure 1: Sketch of the near-surface structure of ion-implanted GaAs before and after laser annealing:

(A) Amorphous surface structure after ion-implantation.

(B) Polycrystalline surface structure after laser annealing with insufficient annealing energy. Arrows represent {100} type directions.

(C) Epitaxial surface structure after laser annealing with sufficient annealing energy.

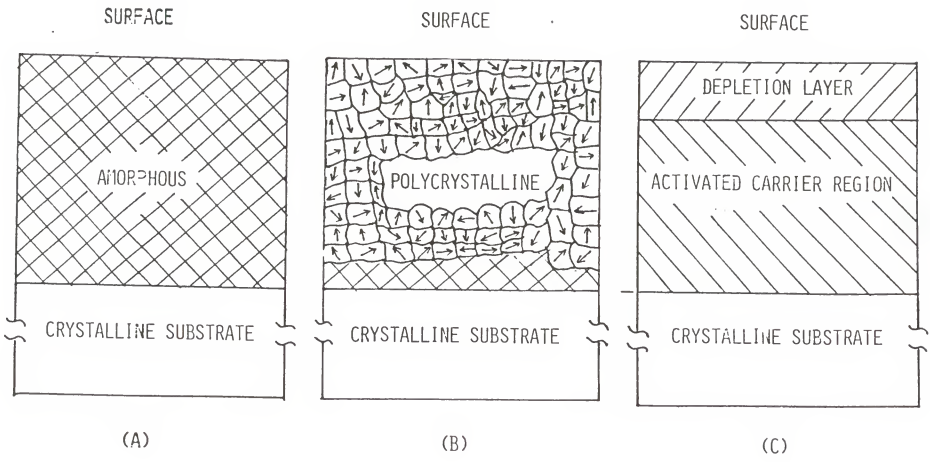
SURFACE
AMORPHOUS
CRYSTALLINE SUBSTRATE
(A)
SURFACE
POLYCRYSTALLINE
CRYSTALLINE SUBSTRATE
(B)
SURFACE
DEPLETION LAYER
ACTIVATED CARRIER REGION
CRYSTALLINE SUBSTRATE
(C)

after pulsed laser annealing for p-type and n-type dopants in GaAs? These are several aspects that need to be studied.

In this thesis, we are going to report the Raman studies of pulsed dye-laser-annealed, implanted GaAs and try to address some of those aspects mentioned above. The implantation doses were in the range of 10^{15} cm^{-2} for both n-type (Sn) and p-type (Cd) dopants at ~100 keV. Therefore the surface structure before laser annealing is amorphous. The GaAs samples were laser annealed with different anneal energies in a wide range. Intensive Raman studies were made on these samples.

The organization of this thesis is as follows: a theoretical sketch of Raman scattering in GaAs and of the origin of the surface depletion layer will be given Chapter 2. The experimental details are discussed in Chapter 3. The results and discussions are presented in Chapter 4. Finally, a brief summary is given in Chapter 5.

Chapter 2

Raman Scattering and the Surface Depletion Layer in GaAs

Origin of the Surface Depletion Layer of Doped GaAs

Because the surface states pin the Fermi level in doped GaAs,[9,10] carrier depletion occurs in the region below the surface. The depleted carriers are trapped in immobile surface states and do not contribute to the electrical conductivity. Therefore, there are no free carriers in this surface depletion layer.

The thickness of the surface depletion layer can be calculated by solving Poisson's equation under the assumption of the Schottky barrier model.[11] Poisson's equation can be simplified to the 1-dimensional case:

$$\frac{d^2\Phi}{dx^2} = \frac{-eN}{K\varepsilon_0} \quad \text{(MKS) for } 0<X<Xn \ .$$

Here Φ is the potential, K is the dielectric constant, ε_0 is the permittivity of free space, N is the density of ionized donors or acceptors and e is the electron charge. X_n is the width of the surface depletion layer. Regard the boundary condition to be

$$\frac{d\Phi}{dx} = 0 \quad \text{at} \quad X=X_n \ .$$

We integrate both side of the Poisson's equation, yielding:

$$\frac{d\Phi}{dx} = \frac{-eN}{K\varepsilon_0}(X-X_n)$$

leading to

$$\Phi = \frac{-eNX_n^2}{2K\varepsilon_0}\left(1 - \frac{X}{X_n}\right)^2 \ .$$

Again here we consider the boundary condition $\Phi=0$ at $X = X_n$. The built-in potential is defined as

$$\Phi_0 = |\Phi(0)| = \frac{eNX_n^2}{2K\varepsilon_0} .$$

Therefore the surface depletion layer width W can be written by rearranging the foregoing equation

$$W = X_n = \left(\frac{2K\varepsilon_0\Phi_0}{eN}\right)^{1/2} .$$

In GaAs the built-in potential Φ_0 is about 0.8 eV.[12] Thus, for example, if $N = \sim 10^{19}/cm^3$, the depletion layer width $W = \sim 100$ Å.

Raman Scattering

Raman scattering is the inelastic scattering of light by phonons. In first-order Raman scattering in crystals, an incident photon of energy $\hbar\omega_L$ is absorbed and a scattered photon of energy $\hbar\omega_S$ is emitted along with the creation or annihilation of a phonon of energy $\hbar\omega_0$. The whole process is governed by the principles of conservation of energy and momentum:

$$\hbar\omega_L = \hbar\omega_S \pm \hbar\omega_0$$
$$\vec{k}_L = \vec{k}_S \pm \vec{q}$$

where $\vec{k}_L$ and $\vec{k}_S$ are the incident and scattered photon wavevectors, $\vec{q}$ is the phonon wavevector. The positive and negative signs correspond to the creation and annihilation of a phonon respectively. The phonon frequency is normally much smaller than that of the photons, ω_L and ω_S for visible light. Therefore we have $|\vec{k}_L| \simeq |\vec{k}_S|$. In the backscattering geometry $\vec{k}_L = -\vec{k}_S$, the phonon wavevector is thus approximately $2|\vec{k}_L|$. In the experiments we report in this thesis, the incident beam was incident at about 45 degrees with respect to the normal direction of the sample surface which was the direction in which we collected Raman signals. Because the index

of refraction is very large in GaAs (it is about 4.6 when the probe wavelength is 457.9 nm.), the angle (inside the crystal) between $\vec{k}_L$ and the normal to the surface is ~9 degrees and therefore it is close to a back-scattering geometry.

Moreover, it is important to point out that since the probe laser wavelength is usually of the order of $5X10^3$ Ångstroms and the lattice size is only of the order of an Ångstrom, the phonon wavevector is much smaller than the Brillouin zone size. E.g., in GaAs, when the probe wavelength λ = 457.9 nm,

$k_L = 2\pi/(\lambda_L/n) = 6.31X10^5\ cm^{-1}$,

$k_S = 2\pi/(\lambda_S/n) = 6.23X10^5\ cm^{-1}$.

Here, n is the index of refraction of GaAs, and λ_S is the wavelength of the scattered light. $\lambda_S = 464.2X10^{-7}$ cm, therefore, $|\vec{k}_L - \vec{k}_S| = |\vec{q}| = 1.25X10^6\ cm^{-1}$. The edge of the Brillouin zone is π/a. Here a is equal to 5.65 Ångstroms in GaAs. So, $\pi/a = 5.56X10^7 cm^{-1}$. Thus the ratio of the phonon wavevector to the Brillouin zone size is about $2.2X10^{-2}$. Therefore the detected Raman phonons are essentially zone-center phonons.

However these consideratinos are entirely different for Raman scattering in amorphous structures (or heavily damaged structures). Wavevector conservation no longer exists. Therefore, in first-order Raman scattering, the Raman phonons are not only zone-center phonons but also phonons all over the Brillouin zone. The Raman spectra then have contributions from all the phonon modes, in contrast to the Raman spectra in a crystal where only zone-center phonons take part.

Raman Measurements in GaAs

GaAs is a zinc-blende structure crystal. Its phonon dispersion curve is shown in Figure 2.[13] For GaAs we have longitudinal (LO) and transverse optical (TO) phonons, and longitudinal (LA) and transverse acoustical (TA)

Figure 2: Phonon dispersion curves of GaAs (Reference 13). T = 296 K. Data points from neutron scattering. Raman scattering occurs from near the Brillouin zone center which is labeled zero on the horizontal axis.

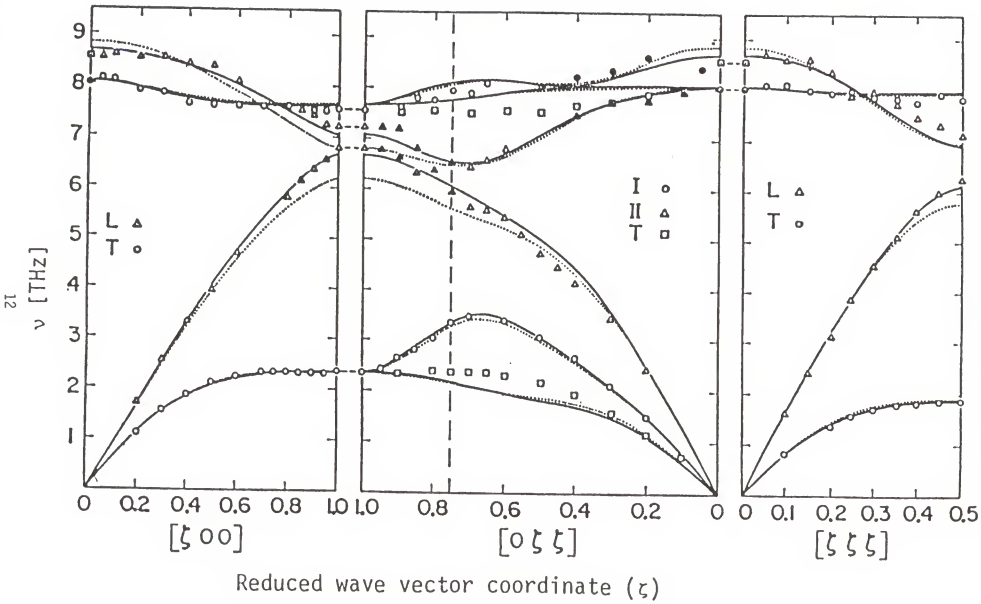
ν [THz]
L △
T ○
I ○
II △
T □
L △
T ○
[ζ 0 0]
[0 ζ 0]
[ζ ζ ζ]
Reduced wave vector coordinate (ζ)

phonons. But because the detected Raman phonons are zone-center phonons and the acoustical phonon frequencies approach zero at the zone center, we can only have LO and TO phonons in Raman scattering in GaAs. Normally, the LO phonon frequency is about 292 cm^{-1} and the TO phonon frequency is about 275 cm^{-1} (or slightly below) at room temperature.

The Raman phonons can interact with the free electrons to form coupled phonon-plasmon modes. In heavily doped GaAs, the coupled LO phonon-plasmon modes are denoted by L^- and L^+. Since the electric field of the LO phonon is heavily screened by the free carriers, the frequency of the LO phonon approaches the TO phonon frequency. This is the L^- mode. The L^- mode has a phonon-like behavior while L^+ is plasmon-like when $N \geq 10^{18}/cm^3$.

The selection rules for LO and TO phonons in the Raman scattering experiment in the backscattering geometry that I report in this thesis are given in Table 1. It is worth noticing that for a (001) sample surface, the LO phonon is allowed in certain scattering configurations while TO scattering should always be forbidden. All these selection rules assume wave-vector conservation and true backscattering.

Figure 3 shows a Raman spectrum of a Cr-doped semi-insulating GaAs crystal (001 surface) where all the free carriers are considered to be trapped. Here X'=[110], Y'=[1$\bar{1}$0]; X =[100], Y =[010], Z =[001]. Only an LO peak at 292 cm^{-1} was detected in the configuration of $Z(X',X')\bar{Z}$ (solid line). In the case of $Z(X',Y')\bar{Z}$, no peak was detected as shown in the curve. All these are consistent with the selection rules given in Table 1. This confirms the fact that the LO peak satisfies the selection rules in the absence of free carriers.

A Raman spectrum of as-implanted GaAs is shown in Figure 4. Because it was heavily damaged by the high dose ion implantation (a dose of $5X10^{15}$ cm^{-2} at 180 keV), this GaAs is considered an amorphous structure. As shown

Table 1: Selection rules for LO and TO phonons in the first-order Raman scattering.

Table 1. Selection rules for LO and TO phonons in the first-order Raman scattering experiment in GaAs reported in thesis.

Scattering configuration $K_i(E_i,E_S)K_S$	Selection rules for first-order Raman scattering assuming wave-vector conservation.
$Z(Y,Y)\bar{Z}$	LO-forbidden TO-forbidden
$Z(X,Y)\bar{Z}$	LO-allowed TO-forbidden
$Z(X',X')\bar{Z}$	LO-allowed TO-forbidden
$Z(X',Y')\bar{Z}$	LO-forbidden TO-forbidden

X=[100], Y=[010], Z=[001].

X'=[110], Y'=[1$\bar{1}$0].

Figure 3: Raman spectrum of semi-insulating Cr-doped GaAs. Polarizations are: (X',X') —— solid line, (X',Y') —— dotted line. X' = [110], Y' = [1$\bar{1}$0].

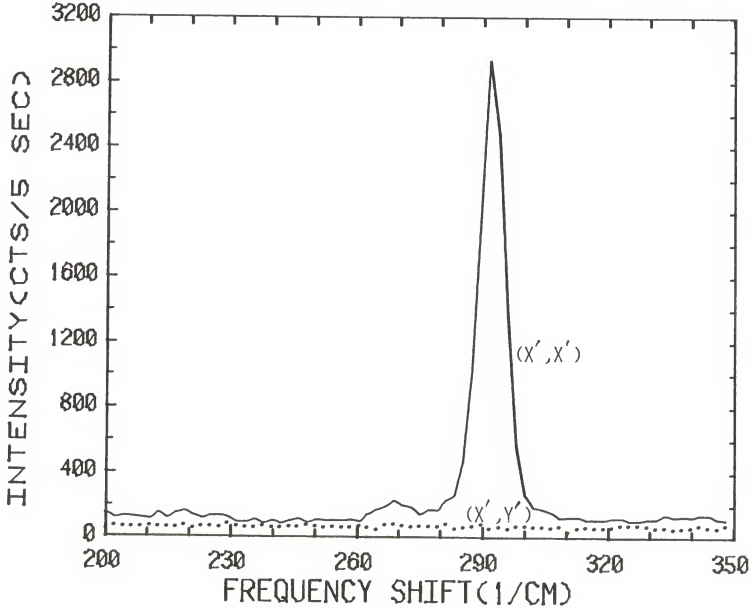
3200
2800
2400
2000
1600
1200
800
400
0
INTENSITY(CTS/5 SEC)
(X′,X′)
(X′,Y′)
200
230
260
290
320
350
FREQUENCY SHIFT(1/CM)

Figure 4: Raman spectrum of as-implanted GaAs.

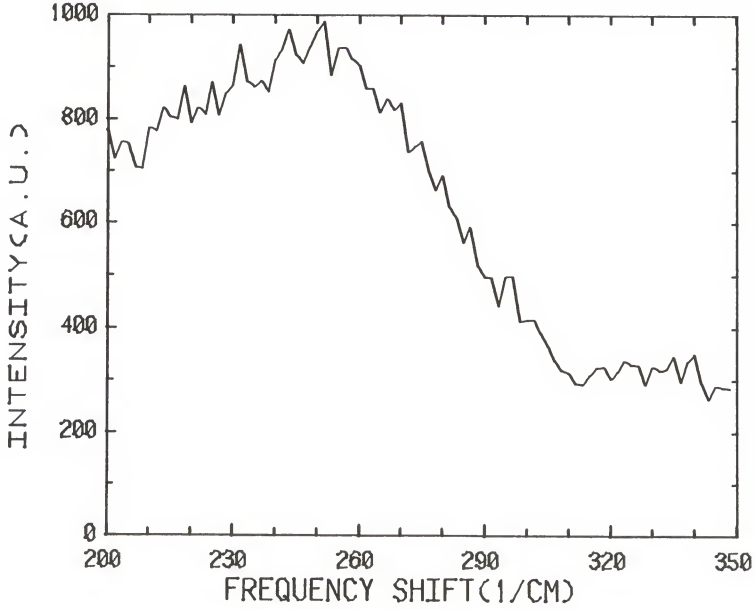
1000
800
600
400
200
0
INTENSITY(A.U.)
200
230
260
290
320
350
FREQUENCY SHIFT(1/CM)

in the spectrum, a broad hump was detected due to the fact that the first-order Raman spectra of amorphous semiconductors contain contributions from all the vibrational modes. The amorphous Raman spectrum is a measurement of the density of vibrational states.

Since the absorption coefficient of GaAs is a function of the wavelength of the incident light, different penetration depths of light can be obtained by using light of different wavelength. Figure 5 gives curves of the light intensity as a function of the distance from the sample surface for light of two different wavelengths.[14] The penetration depth of 514.5 nm is nearly two times as long as that of 457.9 nm. Therefore we can use longer wavelengths to get a deeper Raman probe.

Figure 5: Light intensity in GaAs as a function of the distance from the sample surface for light of two different wave lengths (Ref. 14):
(1) λ = 514.5 nm with absorption coefficient α_1 = 9.034 /micron
(2) λ = 457.9 nm with α_2 = 19.053 /micron.

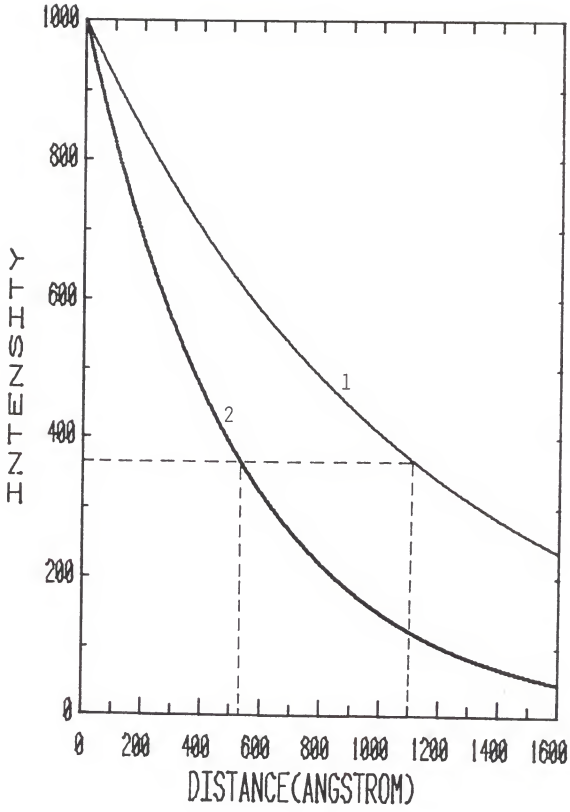
INTENSITY
1000
800
600
400
200
0
0
200
400
600
800
1000
1200
1400
1600
DISTANCE(ANGSTROM)
1
2

Chapter 3

The Experiment

Sample Preparation and Laser Annealing Set-up

Cr-doped semi-insulating GaAs wafers (001 surface) were implanted with Cd ions at 100 keV with doses of $2X10^{15}/cm^3$, $5X10^{15}/cm^3$ and $10X10^{15}/cm^3$ while Si-doped GaAs wafers (Si:$5X10^{17}/cm^3$, 001 surface) were implanted with Sn ions at 180 keV with the same doses. All the implantations were performed at room temperature. Therefore, we have two implantation species prepared for our experiment: Cd, a p-type dopant and Sn, typically an n-type dopant, although potentially amphoteric. The implantation was done in the Department of Physics and Materials Research Institute, University of Missouri—Rolla by Prof. E.B. Hale.

After ion-implantation, a clearly defined, ion-implanted region could be seen on the sample surface because of masking. The samples were attached to a sample plate with mounting wax. The sample plate was then mounted on a translation stage which was driven by two small stepper motors in X and Y directions. The movement of the translation stage was parallel to the sample surface and could be controlled by a PDP 11/34 computer (described later) or manually operated. In this way, we could move the sample horizontally and vertically so as to be able to anneal any place on the sample surface.

We have used a frequency-doubled Nd:YAG (Quanta Ray DCR-1A) pulsed laser of 532 nanometers to pump a dye laser (Lambda-Physik FL-2002) to perform the pulsed annealing at 565 nanometers. The pulse repetition rate was 10 per second while the pulse duration was 10 nanoseconds. Figure 6 shows the schematic diagram of the laser annealing set-up. The laser beam

Figure 6: Pulsed laser annealing set-up. PR = Pellin-Broca prism, M = mirror, F = neutral density filter, L = lens: L_1 (f_1 = 100 cm), L_2 (f_2 = 58 cm), A = aperture, SM = sample mount, BS = beam stop.

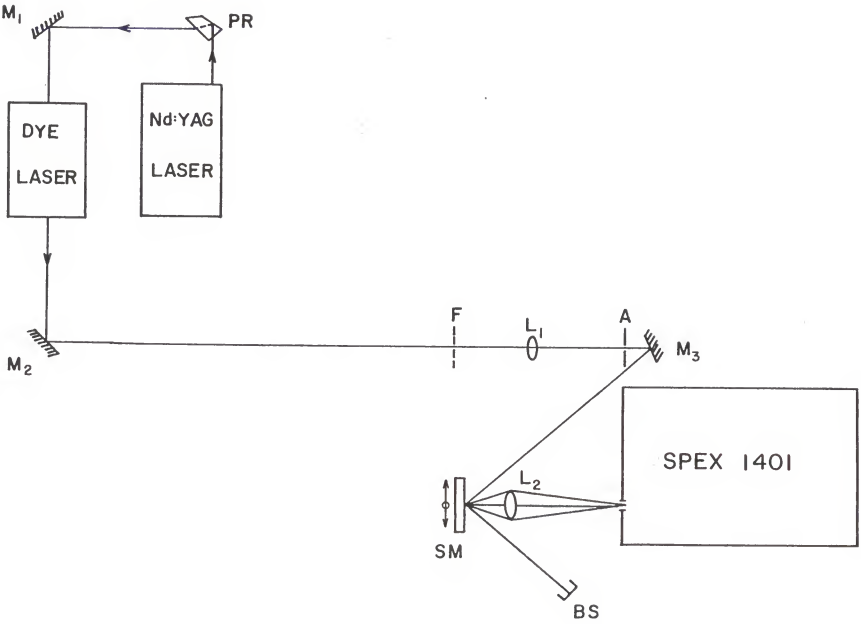
M1
PR
DYE
LASER
Nd:YAG
LASER
M2
F
L1
A
M3
SPEX 1401
L2
SM
BS

was weakly focused by a spherical lens of f=100 cm to a spot diameter on the sample of 0.8 mm which had a smooth, near-Gaussian intensity profile.

Power Density Measurements and Sample Positioning

Pulsed laser energy intensity was measured by using a 200 μm diameter pinhole which was mounted on top of a hole in a flat aluminum plate. The plate was in turn mounted on a translation stage which allowed for horizontal and vertical movement of the pinhole. The annealing laser beam could go through the pinhole plate perpendicularly while it illuminated the sample surface with an incident angle of about 40 degrees. In power measurements, the pinhole was positioned at the sample position and the transmitted beam power was measured by a solar cell (Edmund Scientific) connected to an oscilloscope (Textronix 7904). In order to ensure a linear response of the solar cell, calibrated neutral density filters were placed in the beam to avoid saturation of the detector. The relation between energy per pulse and the voltage measured on the oscilloscope was found by carefully calibrating the solar cell against a disc calorimeter power meter (Scientech Model 3600) which gives the time-averaged power. Since we had already known the repetition rate of the dye laser (10 per second), the energy per pulse could then be related to the voltage of the solar cell. It was found that the response of the solar cell at 565 nanometers was $1.22X10^{-6}$ Joules per volt per pulse. By knowing the area of the pinhole and measuring the energy per pulse going through the pinhole, we were able to calculate the energy density. The power measurements were performed at the beginning and end of the annealing process.

The maximum laser intensity could be found by steering the beam with adjustments on the mirror (M3 in Figure 6) in front of the sample and monitoring the intensity of the radiation transmitted through the 200 μm pinhole. The horizontal and vertical translations of the pinhole were

controlled by micrometers with marks of 10 μm per division. At half maximum power points the diameter of the laser beam was about 800 μm.

In order to ensure that the laser beam illuminated exactly the correct place on the sample, several steps were followed: 1) The pinhole was put at the sample position (see Figure 6). The pinhole plane was positioned near the focal plane of the laser beam. In this configuration, the pinhole and the center of the entrance slit of the spectrometer should be on the optical axis of the collecting lens. The pinhole was moved horizontally and vertically by adjusting the translation stages until its image was centered in the slit of the spectrometer. The image was viewed through a periscope inside the slit with an eyepiece of a magnification of 10. 2) After the pinhole was well positioned, the beam was steered (as mentioned before) to get the maximum power transmission through that pinhole. At this moment, the beam spot was centered on the pinhole while the pinhole was centered in the entrance slit. 3) The pinhole assembly was replaced by a sample assembly (described in the previous section). By sliding the sample assembly along the rail and viewing into the periscope, the sample was positioned when the image of the beam spot fell into the center of the entrance slit of the spectrometer.

The Annealing Process and the Annealed Samples

In the annealing process, neutral density filters were used to control and change the annealing energy densities in a range from 0.057 J/cm^2 to 1.6 J/cm^2. The beam was chopped manually by an aluminum plate in order to get a single shot from a 10 Hz repetition rate laser beam. Labeled energy densities include the cos(40°) factor which is caused by an incident angle of ~40 degrees. After an annealing spot was done, the sample was moved horizontally about 1.5 mm to anneal the next one. Therefore, the single well-separated anneal spots formed a line. When the line was full, the

sample was moved vertically the same distance between two spots in a line to start a new line.

Sample A was a GaAs crystal, Cd-implanted at 100 keV with a dose of $5X10^{15}cm^{-2}$. This sample was annealed with single shot spots in the ion implanted region with energy densities varying from 0.057 J/cm^2 to 1.23 J/cm^2. A sketch of the surface of this sample is shown in Figure 7, while the annealing energy densities of the labeled spots are given in Table 2. The table of Gibbons, et. al[15], gives the projected range of the implanted cadmium ions as 0.0297 microns with the projected standard deviation of 0.0131 microns.

Sample B is a GaAs crystal, Sn-implanted at 180 keV with a dose of $5X10^{15}/cm^2$. The sample was laser annealed at various energy densities ranging from 0.07 J/cm^2 to 1.6 J/cm^2 in the ion-implanted area. In Figure 8 a sketch of the implanted sample surface is given, while the values of the annealing energy densities of the labeled spots are presented in Table 3. From Gibbons, et. al[15], the projected range is 0.0468 microns with the projected standard deviation of 0.0199 microns.

Optical Set-up

We have used a cw Argon laser (Laser Ionics Model 554) to do the Raman scattering. The wavelengths we used for the Raman probe were 457.9 nm and 514.5 nm. As we mentioned in the second chapter, different laser wavelengths have different absorption coefficients in GaAs so that we could get different penetration depths.

Figure 9 gives a schematic diagram of the optics set-up in our experiment. A beam director (BD) which can rotate the image and polarization by 90 degrees was used to rotate the polarization of the laser beam from vertical to horizontal. The beam director consisted of a mirror and a Pellin-Broca prism. The Pellin-Broca prism reflects the beam 90 degrees

Figure 7: Sample A: GaAs crystal, Cd-implanted at 100 kev with a dose of $5X10^{15}$ cm^{-2}. Circular area is the implanted region.

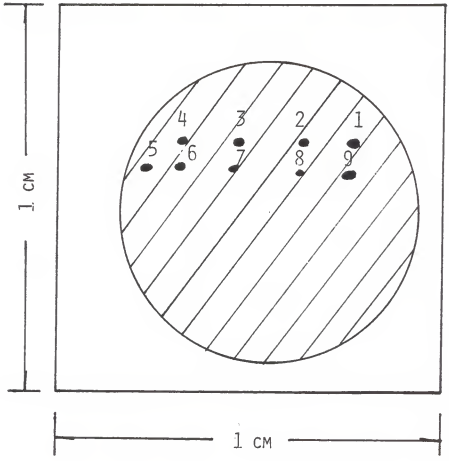
1 cm
1 cm
1
2
3
4
5
6
7
8
9

Table 2: Pulsed laser energy densities of labeled spots on sample A.

Table 2. Pulsed laser energy densities of labeled spots on sample A.

Spot #	Energy density of pulsed laser (J/cm^2)
1	1.23
2	0.88
3	0.61
4	0.43
5	0.3
6	0.21
7	0.11
8	0.08
9	0.056
10	1.23

Figure 8: Sample B: GaAs crystal, Sn-implanted at 180 keV with a dose of $5X10^{15}$ cm^{-2}. Square shaded region is the ion-implanted region.

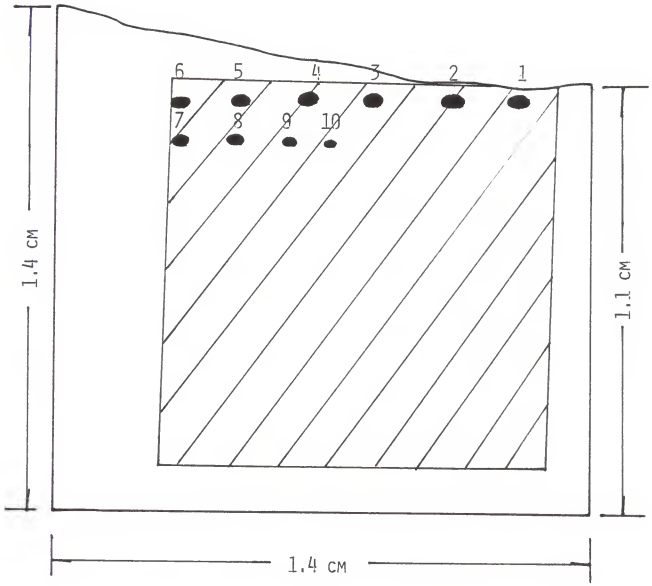
6
5
4
3
2
1
7
8
9
10
1.4 см
1.1 см
1.4 см

Table 3: Pulsed laser energy densities of labeled spots on sample B.

Table 3. Pulsed laser energy densities of labeled spots on sample B.

Spot #	Energy density of pulsed laser (J/cm^2)
1	1.6
2	1.15
3	0.88
4	0.57
5	0.43
6	0.3
7	0.21
8	0.15
9	0.1
10	0.07

Figure 9: Schematic diagram of the optical set-up. BD = beam director, M = mirror, L = lens: L_1 (f_1 = 8.5 cm), L_2 (f_2 = 5.8 cm), L_3 (f_3 = 100 cm), L_4 (f_4 = 12.6 cm), F = filter, A = aperture, P = polarizer, SM = sample mount, SC = scrambler, BS = beam stop.

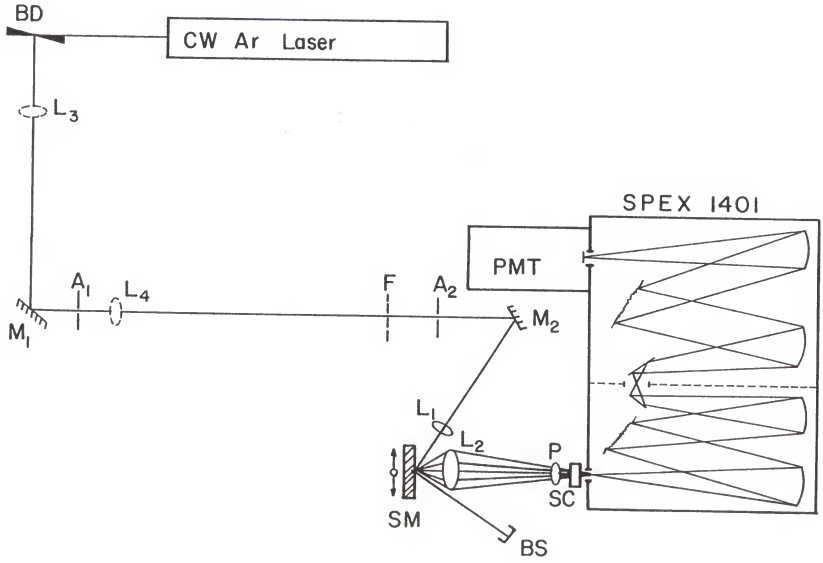
BD
CW Ar Laser
L3
SPEX 1401
PMT
A1
L4
F
A2
M1
M2
L1
L2
P
SC
SM
BS

away from its incident direction. The reason to use the Pellin-Broca prism was to reject the plasma line from the Argon laser. When the Argon laser is used as a Raman source, there are plasma lines in the Raman spectra. These plasma lines are mixed with the Raman signals. In our experiment, at 457.9 nm probe wavelength, there was a strong plasma line at the frequency shift of 274 cm^{-1} that was very near the frequency shift of the TO phonon. A Pellin-Broca prism and aperture with a diameter of ~4 mm were used to minimize the intensity of the plasma line. The prism is made of glass. For glass, the index of refraction is a function of the wavelength of the incident light. Because the plasma line is different in wavelength from the laser line, they are dispersed in different angles. The laser beam coming out of the prism was allowed to pass through the aperture while the plasma line was chopped. It was tested that without using the Pellin-Broca prism, the ratio of plasma line counts to the laser line counts was $1/(6X10^7)$. However, it was about $1/(2.3X10^9)$ by using the prism. Therefore, the plasma line intensity was reduced nearly a factor of 40. A spike filter can also be used to reject the plasma line. It in essence is a piece of glass with multi-layer coating on one side to realize the multiple-beam interference. Therefore, with a fixed incident angle only one kind of wavelength can be transmitted. But the spike causes the loss of nearly 50 per cent of the laser power. Therefore, we preferred using a Pellin-Broca prism since it caused a loss of only ~20 per cent.

A Minolta camera lens (f=5.8 cm) with a large aperture (f/1.4) was used as collecting lens for the Raman signals. In order to match the f-number of the Spex spectrometer (f/6.8), the lens was positioned ~35 cm away from the entrance slit of the spectrometer which gives a magnification of about a factor of 6. The lens was fixed on a transverse fine adjustment stage.

The Probe Beam Measurement

Because the annealing laser beam did not have a flat intensity profile but rather a near-Gaussian intensity profile, the Raman signals coming from different places of the anneal spot were different. Thus a tightly focused probe beam with a ~50 μm diameter spot on the sample surface was chosen compared with a ~800 μm diameter anneal spot (half intensity points). The probe laser beam was focused on the sample surface by a lens of f=8.5 cm (L2 in Figure 9).

Two methods were employed to measure the probe beam spot size on the sample surface. The procedure of the pinhole method was as follows: 1) the sample assembly was replaced by the pinhole assembly (described in the previous section). 2) By adjusting the pinhole assembly, the laser beam was allowed to transmit through a 50 μm diameter pinhole. 3) A solar cell was used to monitor the transmitted beam intensity. The pinhole was moved transversely in the X or Y direction. The half intensity points were considered to define the probe spot diameter. 4) In case the spot diameter was larger than 50 μm, the lens mount of the focal lens (L2) could be translated to move longitudinally along the beam so as to improve the focus to get a smaller spot diameter.

Another beam diameter measurement was made by the periscope method. As we described in the previous section, the image of the spot falling in the center of the entrance slit of the spectrometer was magnified by a factor of ~6. Therefore, a 50 μm diameter spot should have a image spot of ~300 μm diameter in the entrance slit. The image spot could be viewed through the periscope, and the width of the slit was adjusted to fit the image spot diameter. The width of the entrance slit could be read by marks of 2 microns per division on the slit micrometer barrel, and the diameter of the

probe spot could in turn be estimated by dividing the width of the slit a factor of 6.

The pinhole method was more accurate than the periscope method because by that the exact beam diameter of the half intensity can be measured. However, after the optics were well set up, the periscope method was a good one to have a quick estimate.

The Emergency Use of Prof. C.M. Sorensen's Laser

It is worth mentioning that in the middle stage of the experiment, because of the failure of our argon laser (Laser Ionics Model 554), another cw argon laser (Coherent Radiation Model 52) in Prof. C.M. Sorensen's laboratory (room 317 west) was employed. The laser beam was led across three rooms a total distance of about 23 meters to the optical table in our laboratory by reflecting mirrors on the wall and on the table. A polarization rotator was employed to rotate the output laser beam polarization from vertical to horizontal before reflecting by the mirrors on the wall. Thus the direction of the polarization was perpendicular to the plane of incidence of the mirror so that the reflectivity was maximized. Relevant changes were made in the optical set-up. Because of the intrinsic divergence of the laser (~0.8 mrad), the diameter of the laser beam became very large (~30 mm) when it reached the mirror on the optical table after travelling a distance of ~23 meters. This was larger than the size of the Pellin-Broca prism (~15 mm).In order to reduce the beam diameter, two spherical lenses (f_3=100 cm and f_4=12.6 cm) were used to construct a reversed telescope shown as L3 and L4 in Figure 9. The optical distance between L3 and L4 was nearly f_3+f_4 while a Pellin-Broca prism was inserted between them and replaced the mirror M1 to reflect the beam 90^0 from its original direction. The reduced beam spot diameter was ~3.5 mm on the mirror in front of the sample. The rest of the optical set-up remained the

same as described in the previous section. The focused spot on the sample was sometimes not steady because of the air circulation in these rooms where the laser beam was passing. Temperature fluctuations caused fluctuations of the index of refraction in the beam path. This caused the beam deflection. Fortunately, the Raman spectra were not influenced by the unsteady beam spot due to the following reasons: 1) the movement of the beam spot on the sample surface was only ~20 μm and the frequency of vibrations of the spot was high (~5 Hz); 2) a narrow entrance slit of the spectrometer (250 μm) was employed so that most of the time the focused spot was in between the slit and only the signal coming from the desired part of the anneal spot was collected; 3) a fairly long integration time (5 seconds) of the multichannel analyzer was used to collect the signals. Thus, an averaged value of the data was recorded to compensate for the fluctuation of the signals caused by the vibration of beam spot.

Finding the Center of the Anneal Spot

As pointed out in the previous section, the Raman signals coming from different places of the anneal spot were different. Therefore, it was very important to find the center of the anneal spot. Since the anneal spots were very small (~800 μm diameter), it was very unreliable to find the center of the spots by our eyes. Therefore, a method of spatial scanning was employed.

The spatial scan was made by a computer controlled, stepper-motor-driven stage. A computer program DRIVEM.MAC (see Appendix) was used to control the movement of the motor. The sample could be moved step by step in either X or Y directions. Each step was 50 microns since the Raman probe beam spot was 50 microns in diameter. The program DRIVEM.MAC could drive the sample forward or backward in horizontal and vertical directions.

For convenience, we called the movement of forward and backward in horizontal direction as DRIVEX and REVESX respectively; Similarly, we used programs called DRIVEY and REVESY in the vertical direction. Moreover, the program allowed us to choose how many steps the sample should move and how many seconds the sample should wait between two steps. The following procedure for doing a spatial scan was followed: 1) the probe laser spot was set on the anneal spot manually. 2) A horizontal spatial scan was employed (DRIVEX). The number of steps to be moved were 30 and the time duration between two steps was 4 seconds. 3) The spectrometer was set at the LO phonon position (292 cm^{-1}) and the integration time of the multichannel analyzer (MCA) was 4 seconds as well. Therefore, each channel of the MCA was related with one step movement of the sample. 4) The spatial scan and the data collection were started at the same time.

Figure 10 shows a plot of a spatial scan. A complete spatial scan allowed the laser beam to move across the spot a distance of 1500 microns. This was large enough to cover a spot. The center of the spot could be found on the spatial scan plot (position a in Figure 10) usually from symmetry considerations. The channel number of the center of the spot on MCA indicated the number of steps moved from the beginning by the motor. The program DRIVEM was used to have a quick drive to the center of the spot found in DRIVEX. However, the center found in DRIVEX may not be the center in DRIVEY. Therefore, a spatial scan in the vertical direction (DRIVEY) was used. The procedures of DRIVEY were exactly the same as those of DRIVEX. If the center found in DRIVEY was not the center found in DRIVEX, a scan of DRIVEX was repeated. In this way, the center of the spot was found by repeating DRIVEX and DRIVEY until the center found in DRIVEX overlapped the center found in DRIVEY.

Figure 10: Spatial scan profile of an anneal spot.
Probe laser wavelength λ = 457.9 nm,
X' = [110], slit width: 500-600-500 μm.

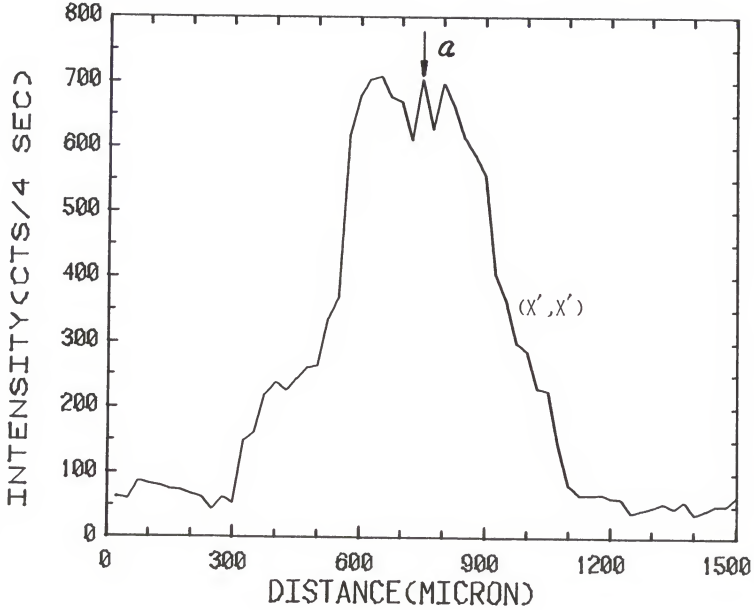
800
700
600
500
400
300
200
100
0
INTENSITY(CTS/4 SEC)
a
(X',X')
0
300
600
900
1200
1500
DISTANCE(MICRON)

Signal Detection and Raman Data Acquisition

Figure 11 gives a schematic diagram of the signal collection and data acquisition system. The Raman signal was analyzed with a double spectrometer (Spex Model 1401). Gratings of 1180 grooves/mm were employed. In order to get good resolution, the width of both entrance and exit slits were 250 μm while the intermediate slit was 600 μm (250-600-250). The height of the entrance slit was 2 mm. With these settings, the resolution of the spectrometer was ~7 cm^{-1}. A photomultiplier tube (ITT FW-130) with an S-20 cathode was cooled down to -20°C thermoelectrically in a tube housing to reduce the dark current to about 5 counts per second. Pulses from the PMT tube were amplified, discriminated, and shaped, and then sent to a multichannel analyzer (Canberra Model 8100A) to record the digital data. Meanwhile a frequency counter (Hewlett-Parkard) was employed to monitor the signal visually.

In order to record Raman signals for different polarizations, a polarizer was used in front of the entrance slit of the spectrometer. Figure 12 shows the spectral response of the PMT detector along with the spectrometer (Spex 1401) which was equipped with a pair of gratings of 1180 grooves/mm. A tungsten standard lamp (L-101, Electrooptic Associates) was employed as a white light source. The spectrometer was scanned from 400 nm to 800 nm. The lamp was positioned 100 cm away from the entrance slit of the Spex along the axis of the collecting lens. The optical set-up remained the same except the sample mounting was replaced by a pinhole apparatus. Because the spectrometer had quite different response for horizontally and vertically polarized signals, a scrambler was used right after the polarizer to reduce the response difference between horizontally and vertically polarized signals (Figure 13). The residual response difference of the two polarizations and the small oscillations as shown in

Figure 11: Signal detection and data acquisition system. M = mirror, A = aperture, L = lens, SM = sample mount, BS = beam stop.

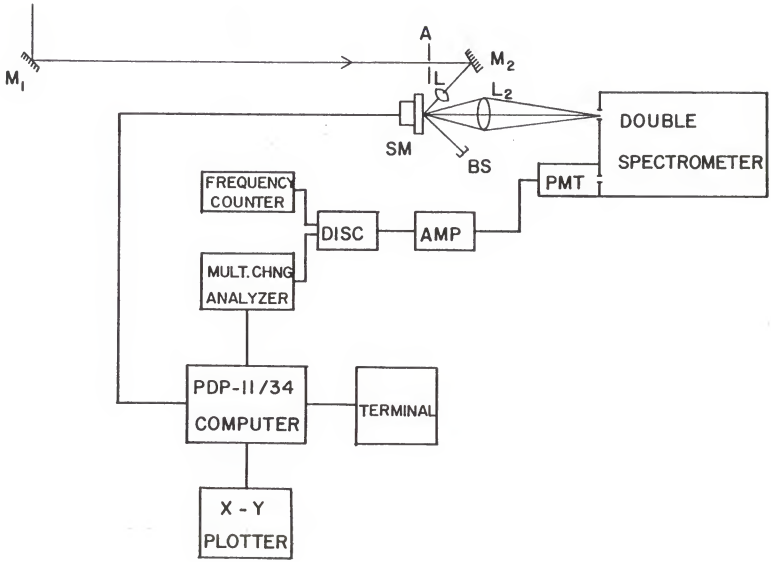
A
M2
M1
L
L2
SM
BS
DOUBLE
SPECTROMETER
PMT
FREQUENCY
COUNTER
DISC
AMP
MULT. CHNG
ANALYZER
PDP-11/34
COMPUTER
TERMINAL
X - Y
PLOTTER

Figure 12: Spectral response of the ITT FW 170 photomultiplier and spectrometer (Spex 1401) for two polarizations. Note that the reponses of two polarizations are quite different. Spectrometer grating: 1180 grooves/mm. A tungsten standard lamp (L-101, Electrooptic Associates) was used.

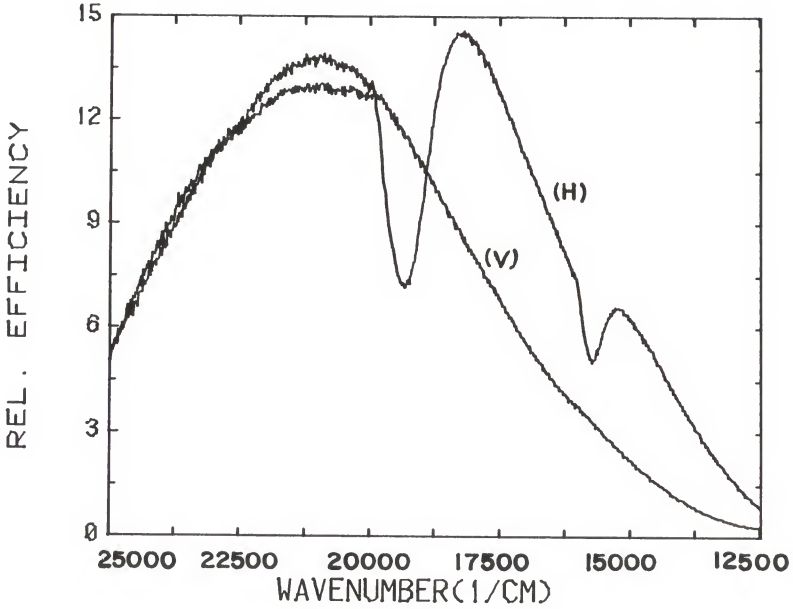
15
12
9
6
3
0
REL. EFFICIENCY
(H)
(V)
25000
22500
20000
17500
15000
12500
WAVENUMBER(1/CM)

Figure 13: Spectral response of the ITT FW 170 photomultiplier and spectrometer (Spex 1401) with a scrambler in front of the entrance slit. Note that the reponses of two polarizations are now similar.

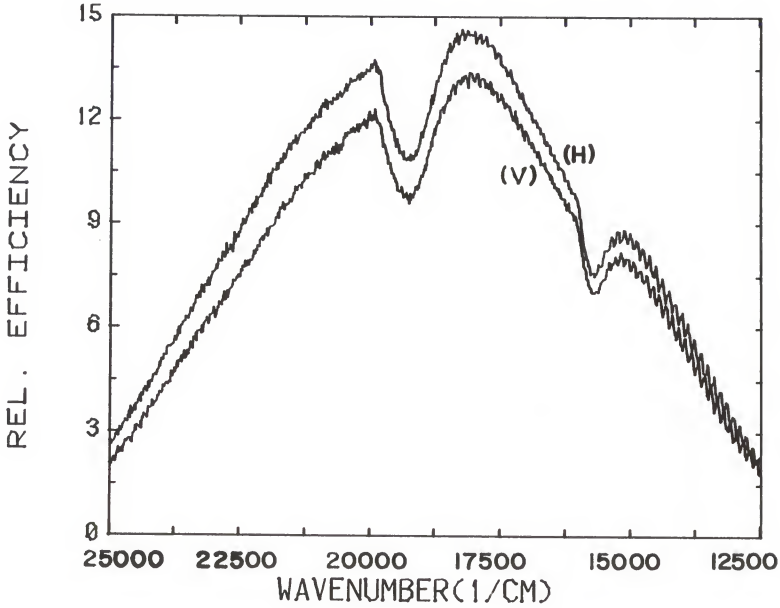
15
12
9
6
3
0
REL. EFFICIENCY
(H)
(V)
25000
22500
20000
17500
15000
12500
WAVENUMBER(1/CM)

Figure 13 can be explained by the possibility that 1) the scrambler was slightly misoriented, and 2) the scrambler was not fully illuminated.

After a complete scan through the Raman peaks was finished, the digital data were transferred from multichannel analyzer to a disk in the PDP 11/34 computer. A plotted data curve could be obtained thereafter by an interactive digital plotter (Tektronix Model 4662) connected to the computer.

Chapter 4

Results and Discussion

As discussed in Chapter 1, two kinds of implantation species were prepared for the experiment: n-type (Sn implanted) and p-type (Cd implanted) GaAs. Experimental results for these two species will be presented and discussed respectively and be compared with each other.

Raman spectra were obtained with the 457.9 nm and 514.5 nm probe beams of an Ar^+ laser with typically a power of 100 mW at an incident angle of 45 degrees. The polarization of the incident laser light was parallel to the horizontal incident plane so as to minimize the reflectivity and maximize the Raman signal. Scattered light was analyzed for both horizontal and vertical components. Incident and scattered polarizations, except where indicated otherwise, were denoted (X',X') and (X',Y') where X'=[110] and Y'=[1$\bar{1}$0].

Sn-implanted Sample

Figure 14 shows the Raman spectra obtained at the wavelength of 457.9 nm for a series of laser anneal energy densities from sample B, which is implanted with $5X10^{15}/cm^2$ Sn ions at 180 keV. The spectra show an abrupt transition between annealing energies of 0.21 J/cm^2 and 0.3 J/cm^2. At 0.21 J/cm^2 and below, two peaks are observed at the LO and TO positions respectively in both scattering configurations (X',X') and (X',Y'). As mentioned in Chapter 2, in Raman scattering from a (001) surface of GaAs only LO phonons are normally allowed. Thus, the peak at the TO position arises from polycrystalline grains not having (001) surface orientation. The abrupt disappearance of the TO-like peak near 270 cm^{-1} at 0.3 J/cm^2 is a clear indication that epitaxial regrowth has occurred.

Figure 14: Raman spectra (λ = 457.9 nm) of Sn-implanted GaAs with dose of $5X10^{15}$ cm^{-2} for several anneal energies. Spectrometer resolution of 7 cm^{-1} is shown by vertical bars in upper left. Polarizations are shown as: (H,H) - solid curve, (H,V) - dotted curve. H = [110], V = [1$\bar{1}$0].

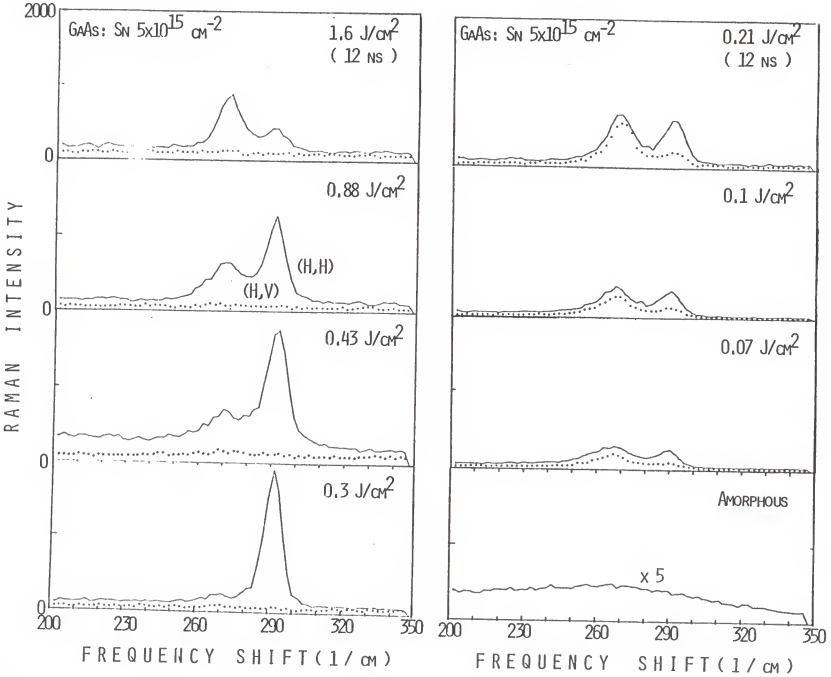
GaAs: Sn 5x10^15 cm^-2
1.6 J/cm^2
(12 ns)
0.88 J/cm^2
(H,H)
(H,V)
0.43 J/cm^2
0.3 J/cm^2
2000
0
RAMAN INTENSITY
200
230
260
290
320
350
FREQUENCY SHIFT(1/cm)
GaAs: Sn 5x10^15 cm^-2
0.21 J/cm^2
(12 ns)
0.1 J/cm^2
0.07 J/cm^2
Amorphous
x 5
FREQUENCY SHIFT(1/cm)

At 0.3 J/cm^2 and above, the LO-like mode at ~292 cm^{-1} gradually decreases in strength with increasing anneal energy. This indicates that it originates in a surface depletion layer which is decreasing in thickness due to increasing carrier activation with increasing anneal energy.

In contrast to the LO peak, the TO-like mode at ~272 cm^{-1} increases in strength with increasing anneal energy above 0.3 J/cm^2. Its polarization characteristics are consistent with that of the L^- component of the LO phonon-plasmon modes originating in the region of high carrier activation below the surface depletion layer. Therefore, both peaks indicate gradually increasing carrier activation with pulsed laser anneal energies up to a factor of four above the epitaxial regrowth threshold. Such behavior has also been noted in picosecond pulse annealing of InP.[16]

For electron concentrations above ~5X10^{17}/cm^3 the position of the L^- mode is insensitive to carrier concentration and is located at the fully screened value equal to the normal TO position (272 cm^{-1}). A clear indication of the free carrier densities can be obtained from observations of the position of the L^+ mode in Raman scattering.[17] We have not found such a peak in sample B by using laser wavelengths of either 457.9 nm or 514.5 nm. However comparison of the relative peak heights from the 1.6 J/cm^2 anneal spot with spectra from bulk doped samples indicates a carrier density slightly above 1X10^{19}/cm^3.

It can be observed from the spectra below 0.3 J/cm^2, that the polarization behavior of the LO-like peak near 290 cm^{-1} is different from that of the TO-like mode at ~270 cm^{-1}. This is consistent with the impurity-induced Fröhlich coupling mechanism.[18,19] This Fröhlich electron-phonon coupling produces diagonal scattering, i.e., $e_s||e_i$ independent of sample orientation. In order to verify this behavior, sample B was rotated 45 degrees about its normal so that X=[100],Y=[010] and found also in this

case (X,X) scattering exceeds (X,Y) scattering (Figure 15). Note that the normally allowed Raman scattering would require (X,Y) scattering in this case. Similar results have been found for LO peaks in heavily doped p-GaSb and p-InSb.[19]

The ratio of peak heights of TO-like to LO-like modes is a strong function of the laser penetration depth. Figure 16 shows the spectra from 0.43 J/cm^2 anneal spot with 514.5 nm and 457.9 nm on sample B. It indicates that with 514.5 nm excitation the L^- peak is enhanced because of the deeper light penetration. Both wavelengths indicate a depletion width of ~100 Å which on a simple Schottky-barrier model[11,19] requires a carrier concentration of ~$2X10^{19}/cm^3$ as shown in Chapter 2.

A spatial scan was employed as described in Chapter 2, to find the center of the anneal spot. In fact, more information can be obtained from the spatial scans. Figure 17 gives examples of spatial scans (DRIVEX) of two anneal spots. The spectrometer was fixed at the LO phonon position (292 cm^{-1}) and the TO phonon position (268 cm^{-1}) for two scattered polarizations. From the spatial scans, it is easy to find the diameter of the anneal spot (~800 μm) and the region of epitaxy (e.g. ~350 μm for 0.57 J/cm^2 anneal spot). It indicates a polycrystalline structure near the edge of the spot and epitaxial regrowth in the center region. If spatial scans in both directions (horizontal and vertical) are given, a two-dimensional picture can be obtained for the structure of the material and the Raman signals.

Cd-implanted Sample

The activation of p-type ion-implanted dopants in GaAs whether by conventional thermal annealing or by pulsed laser annealing is easier than that for n-type dopants. The projected range of 100keV Cd ions in GaAs is approximately 30 nm[15]. Therefore, for a dose of $5X10^{15}$ cm^{-2} the peak

Figure 15: Raman spectra (λ = 457.9 nm) of two annealed spots (0.88 J/cm^2 and 0.21 J/cm^2). Note that (B) and (D) are spectra where sample has been rotated by 45 degrees so that the solid curve is (X,X) and dotted curve is (X,Y). X = [100], Y = [010].

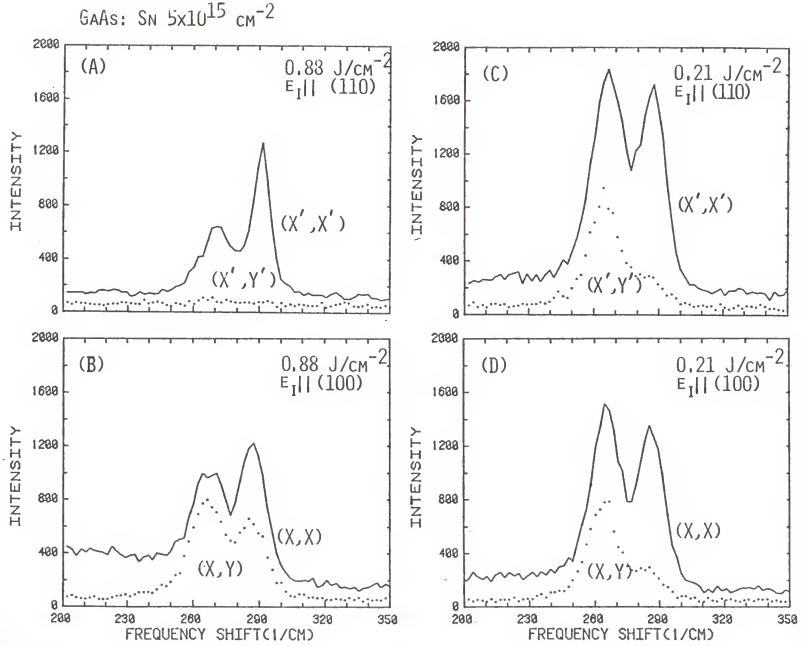
GaAs: Sn 5x10^15 cm^-2
(A)
0.88 J/cm^-2
E_I|| (110)
(X',X')
(X',Y')
(C)
0.21 J/cm^-2
E_I|| (110)
(X',X')
(X',Y')
(B)
0.88 J/cm^-2
E_I|| (100)
(X,X)
(X,Y)
(D)
0.21 J/cm^-2
E_I|| (100)
(X,X)
(X,Y)
INTENSITY
FREQUENCY SHIFT(1/CM)
0
400
800
1200
1600
2000
200
230
260
290
320
350

Figure 16: Raman spectra of 0.43 J/cm^2 anneal spot of the 514.5 nm and 457.9 nm probes on sample B. Spectrometer resolution of 7 cm^{-1} is shown by vertical bars in the upper left. Polarizations are shown as: (H,H) - solid curve, (H,V) - dotted curve. H = [110], V= [1$\bar{1}$0].

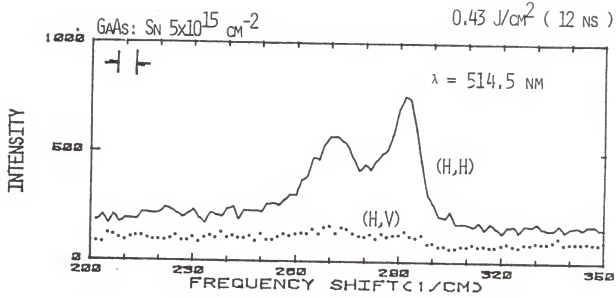
GaAs: Sn 5x10^15 cm^-2
0.43 J/cm^2 (12 ns)
λ = 514.5 nm
(H,H)
(H,V)
INTENSITY
1000
500
0
200
230
260
290
320
350
FREQUENCY SHIFT(1/CM)

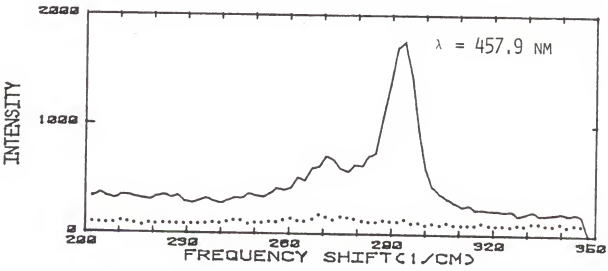
λ = 457.9 nm
INTENSITY
2000
1000
0
200
230
260
290
320
350
FREQUENCY SHIFT(1/CM)

Figure 17: Raman spatial scans (λ = 457.9 nm) of the two anneal spots on sample B (GaAs: Sn $5X10^{15}$ cm^{-2}) with spectrometer fixed at the LO phonon position (268 cm^{-1}) for two scattered polarizations (e_s || X' and e_s || Y'). The spectrometer slit width is 500-600-500 μm.

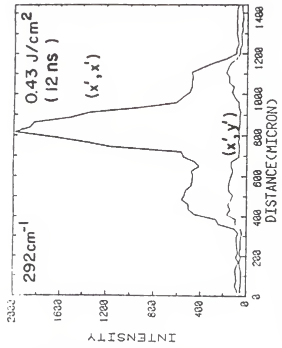
292cm^{-1}
0.43 J/cm^2
(12 ns)
(x',x')
(x',y')
INTENSITY
0
400
800
1200
1600
2000
0
200
400
600
800
1000
1200
1400
DISTANCE(MICRON)

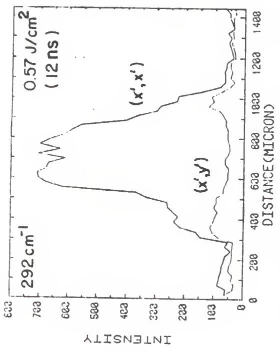
292cm^{-1}
0.57 J/cm^2
(12 ns)
(x',x')
(x',y')
INTENSITY
0
100
200
300
400
500
600
700
800
0
200
400
600
800
1000
1200
1400
DISTANCE(MICRON)

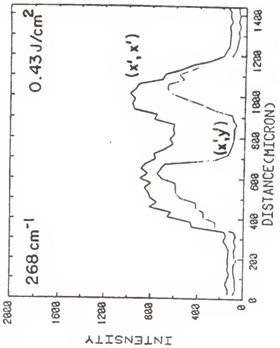
268 cm^{-1}
0.43 J/cm^2
(x',x')
(x',y')
INTENSITY
0
400
800
1200
1600
2000
0
200
400
600
800
1000
1200
1400
DISTANCE(MICRON)

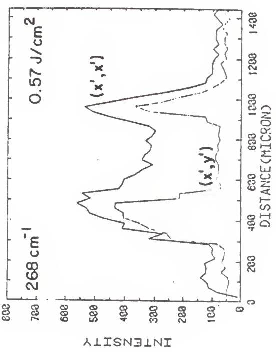
268 cm^{-1}
0.57 J/cm^2
(x',x')
(x',y')
INTENSITY
0
100
200
300
400
500
600
700
800
0
200
400
600
800
1000
1200
1400
DISTANCE(MICRON)

impurity density before annealing should be ~$1\text{-}2\times10^{21}/cm^3$. For near-threshold pulsed annealing, where the liquid phase just penetrates beyond the amorphized layer, little additional dopant diffusion is expected and thus there should be a similarly high dopant density after annealing. However for higher pulse anneal energies significant ion-diffusion may be expected and consequently lower dopant densities. Free carrier concentrations may be less if large numbers of dopant ions are electrically inactive.

Figure 18 shows the Raman spectra of sample A, Cd-implanted GaAs, covering a wide range of anneal energies. The spectra are dominated by one broad peak located near the TO phonon position in undoped GaAs. As mentioned before, in Raman scattering from a (001) surface of GaAs, TO phonons are not allowed in the backscattering geometry. Therefore, scattering at this position may indicate poor epitaxial regrowth, i.e., a polycrystalline surface region as discussed above in the case of sample B (n-type GaAs) at energy densities below ~0.3 J/cm^2. However, at higher anneal energies, I believe the forbidden TO-phonon Raman scattering is induced by wave-vector nonconservation brought about in the Raman process by the presence of impurities.

A very interesting point is that the peaks due to completely screened LO modes show the same self-energy effects seen for the TO phonons. A peak shift to low energies and a peak broadening were measured for TO phonons of our heavily ion-implanted p-type GaAs samples similar to that identified for heavy Zn-doped GaAs[18] in Raman-allowed configurations. These self-energy effects are the result of a deformation-potential-type interaction between the TO phonon (or in this case the completely screened LO phonon) and a Raman-active continuum of indirect transitions within the heavy-hole valence band.[18]

Figure 18: Raman spectra (λ = 457.9 nm) of Cd-implanted GaAs with a dose of $5X10^{15}$ cm^{-2} for four different pulsed laser anneal energies. Polarizations are as follows: (X',X') - solid curve, (X',Y') - dotted curve. X' = [110], Y' = [1$\bar{1}$0]. Spectrometer resolution of 7 cm^{-1} is shown by vertical bars in the upper left. Dashed vertical line at 262 cm^{-1} indicates the peak position near the epitaxial regrowth threshold.

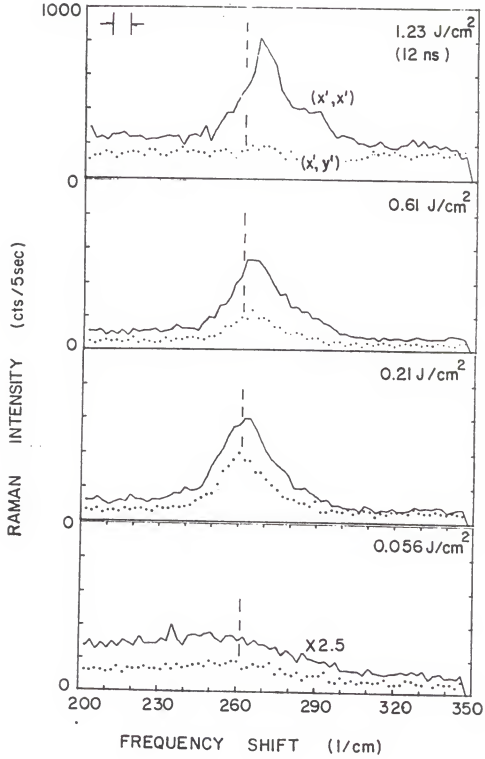
1000
1.23 J/cm2
(12 ns)
(x', x')
(x', y')
0
0.61 J/cm2
0
0.21 J/cm2
0
0.056 J/cm2
X2.5
0
200
230
260
290
320
350
RAMAN INTENSITY (cts/5sec)
FREQUENCY SHIFT (1/cm)

At carrier densities of $4X10^{19}/cm^3$ and above, Olego & Cardona[18] interpreted the peak at the TO phonon position as arising from the L^- modes of the completely screened LO phonons. Normal polarization selection rules of the LO phonon are invalidated because an ionized impurity-induced wave-vector-nonconserving mechanism dominates the Raman scattering efficiency. In Zn-doped GaAs the phonon frequency decreased monotonically and the width of the peak increased with increasing Zn density up to the doping limit of $9X10^{19}/cm^3$. The peak shift and broadenings we observed were still larger. Thus at 0.3 J/cm^2 the TO-like peak is shifted 10 ± 2 cm^{-1} below its normal position in undoped GaAs. This compares with a maximum shift of $-5cm^{-1}$ observed in Reference 18 for a sample with a hole concentration of $9X10^{19}/cm^3$. Similarly the linewidth observed for this spot is 17 ± 2 cm^{-1} which again suggests ionized acceptor concentrations well above $1X10^{20}/cm^3$. However as annealing energy is increased the Raman peak frequency shift rises and the linewidth decreases indicating reduced carrier concentrations. At 1.2 J/cm^2 the shift of -3 cm^{-1} and width of $\sim8cm^{-1}$ are both consistent with carrier concentrations in the mid-10^{19} range.

Results obtained on samples with the lower implantation dose ($2X10^{15}/cm^2$) and the higher dose ($1X10^{16}/cm^2$) exhibit qualitatively similar annealing behavior. The data indicate low activation of Sn dopants (a maximum of ~2% activation) but clearly show increasing activation with annealing fluences well above the epitaxial threshold. Cd implants appear to be activated easily to densities near $10^{21}/cm^3$. The behavior of the Raman spectra appear to follow the trends observed in heavy Zn-doped GaAs.

Chapter 5

Summary and Conclusions

Raman scattering has proved to be a very useful nondestructive technique for studying doped GaAs over a broad range of carrier concentrations. This technique was used here to study the annealing behavior produced by 10 nsec, 565 nm dye laser pulses in high-dose ion-implanted GaAs. Laser lines of 457.9 nm and 514.5 nm of a cw Ar^+ laser were employed to do the Raman probing. The Raman spectra indicate that the threshold of epitaxial growth for GaAs lies between 0.2 and 0.3 J/cm^2. The study of the Raman spectra provides a first qualitative estimate of the degree of electrical activity. The results of this study indicate a vast difference in pulsed laser annealing behavior between the n-type (Sn) and p-type (Cd) dopants in GaAs.

By comparing with the trends observed in heavy Zn-doped GaAs, we estimate, for p-type dopant (Cd) in GaAs, that the carrier activation probably exceeds $1X10^{20}/cm^3$ ($\geq$50%) at low energy density annealing ($\leq$0.3 J/cm^2), with no indication of a surface depletion layer. However carrier activation decreases as the annealing energy increases. More precise estimates of carrier activation are not possible at this point since Raman data on extremely heavily doped p-type GaAs are available only for Zn doping and only up to hole concentrations of $9X10^{19}/cm^3$. The possible dependence of ionized impurity scattering on dopant specie is presently unknown. Furthermore the behavior of peak shift, width and polarization is unknown for dopant densities above $1X10^{20}/cm^3$.

For n-type (Sn-implanted) dopants in GaAs, the annealing behavior follows trends observed with conventional doping techniques, e.g., it is much more difficult to obtain high carrier activation than for p-type

dopants. Thus, available Raman data in that literature[20] are limited to samples with electron concentrations of $1.6X10^{19}/cm^3$. The lack of data at higher electron concentration makes definitive interpretation of the Raman spectra difficult but several features can be identified.

The behavior of the spectra is more complex than the case of the Cd-implanted sample. This behavior may be related to the potentially amphoteric nature of Sn as a dopant in GaAs and the difficulties of achieving high carrier activation of species such as Sn or Si which are typically n-type. The Raman spectra depend strongly on the annealing pulse energy density between 0.07 J/cm^2 and 1.6 J/cm^2 with evidence of an L^- coupled mode, a surface depletion layer, and increasing carrier activation from energy densities of 0.3 J/cm^2 through 1.6 J/cm^2. Best carrier activation is obtained at 1.6 J/cm^2 with a carrier concentration estimated to be slightly above $1X10^{19}/cm^3$ (~2% activation). It appears a trend that higher carrier activation can be achieved with higher annealing energy density for Sn implants. The present work has not shown an upper limit to the optimum laser annealing energy for the Sn-implanted samples. Higher pulse energies were not used because of plasma formation at the sample surface during the laser pulse and visual evidence of a textured (rippled) surface at these high energies.

Some preliminary experiments were performed with multiple pulses at low anneal energy above and below the epitaxial threshold respectively. Figure 19 shows the Raman spectra of the single and multiple-pulse annealing of 0.085 J/cm^2 and 0.42 J/cm^2 on sample B. The spectra indicate that with pulse anneal energy below the epitaxial threshold (see spectra of (A) and (B)), the multiple-pulse annealing effect of 1000 pulses at 0.085 J/cm^2 is similar to that of a single pulse at 0.21 J/cm^2 (Figure 14). After multiple-pulse annealing, the intensity of the LO and TO-like peaks

Figure 19: Raman spectra (λ = 457.9 nm) of multiple-pulse anneal spots on sample B. Spectrometer slits are 250-600-250 μm. Polarizations are as: (H,H) - solid curve, (H,V) - dotted curve. H = [110], V = [1$\bar{1}$0].

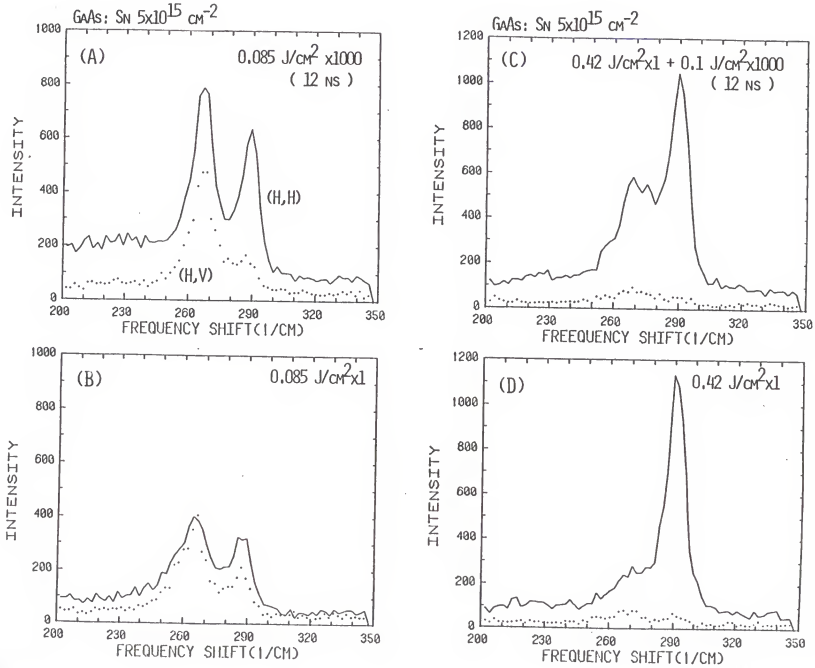
GaAs: Sn 5x10^15 cm^-2
(A)
0.085 J/cm^2 x1000
(12 ns)
(H,H)
(H,V)
INTENSITY
FREQUENCY SHIFT(1/CM)
(B)
0.085 J/cm^2x1
(C)
0.42 J/cm^2x1 + 0.1 J/cm^2x1000
(D)
0.42 J/cm^2x1

increase with (X',X') scattering and the ratio of the intensity of the peak at TO position with (X',Y') scattering to that with the (X',X') scattering decreases. This indicates the trend of removing the damage of the crystal. The effect of the 1000 pulses at the low energy density of 0.1 J/cm^2 after a single pulse annealing of 0.42 J/cm^2 (spectrum (C)) is equivalent to that of the single pulse annealing at 0.88 J/cm^2 (Figure 14). An increase in the intensity of the L^- peak suggests that better carrier activation may be achieved.

In general, the effects of multiple-pulse annealing on Sn-implanted GaAs at fairly low pulse energies appear to be equivalent to that of single pulse annealing at higher energies. Therefore, further studies on multiple-pulse annealing on GaAs is suggested.

APPENDIX

Program listing of DRIVEM

```
DRIVEM.MAC
                ;PROGRAM TO DRIVE THE STEPPING MOTOR TO HAVE A
                ;VERTICAL OR HORIZONTAL SCAN  ON THE SAMPLE.
        .MCALL  .TWAIT, .EXIT, .TTYIN, .PRINT

        MOV     R0, BUFF

START:  CLR     R0
        CLR     R1
        .PRINT  #MESS2
        JSR     PC, TYIN
        MOV     R0, CHL
        CMP     CHL, #1
        BNE     LOOK1
        MOV     #PAR1, J
        MOV     #20 , L
        BR      CON
LOOK1:  CMP     CHL, #2
        BNE     LOOK2
        MOV     #PAR2, J
        MOV     #100,  L
        BR      CON
LOOK2:  CMP     CHL, #3
        BNE     LOOK3
        MOV     #PAR3, J
        MOV     #40, L
        BR      CON
LOOK3:  CMP     CHL, #4
        BNE     END
        MOV     #PAR4, J
        MOV     #200,  L
        BR      CON
END:    .EXIT

CON:    CLR     R1
        .PRINT  #MESS2
        JSR     PC, TYIN
        MUL     #60., R0
        MOV     R1, TIME+2

        CLR     R1
        .PRINT  #MESS1
        JSR     PC, TYIN
        MOV     R0, STEP

        MOV     #20,@DZCSR      ;CLEAR CSR
1$:     BIT     #20,@DZCSR      ;TESTS TO SEE IF CLEAR IS EXECUTED
        BNE     1$              ;RETURNS TO 1$ IF CLEAR IS STILL
                                ;BEING EXECUTED
        MOV     J,@DZLPR        ;IDENTIFIES LINE
        MOV     L,@DZTCR        ;LOADS WORD
        MOV     #40,@DZCSR      ;RELEASES WORD
2$:     TST     @DZCSR          ;TESTS BIT 15(TRANSMIT READY)
        BPL     2$              ;WAITS UNTIL TRANSMIT IS COMPLETE
        CLR     R0
        CLR     R1              ;THIS SECTION IS USED TO TRANSLATE
                                ;THE STEPPING MOTOR AT A CERTAIN RATE
REPT:   MOV     #125,@DZTBUF    ;SENDS SIGNAL (2 PULSES/WORD =5MICROMS)
3$:     TST     @DZCSR
        BPL     3$
        INC     R0
        CMP     #4,R0
        BGT     REPT
        .TWAIT  #TAREA,#TIME    ;WAITE FOR (OPTION) SECONDS
        CLR     R0
```

```
        INC     R1
        CMP     STEP,R1
        BGT     REPT
        .EXIT
MESS1:  .ASCIZ  /TYPE NUMBER OF STEPS TO BE MOVED.>/<200>
        .EVEN
MESS2:  .ASCIZ  /TYPE NUMBER OF SECONDS BETWEEN TWO STEPS.>/<200>
        .EVEN
MESS3:  .ASCIZ /TYPE 1,2,3,OR 4 FOR DRIVEX, PVERSX, DRIVEY, OR PVERSY.>/<200>
        .EVEN

TAPEA:  .BLKW   5
TIME:   .WORD   0,60.
STEP:   .WORD   0
BUFF:   .WORD   0
CHL:    .WORD   0

TYIN:   MOV     DATA, R1
        CLR     R2
INLOOP: .TTYIN  (R1)+
        INC     R2
        CMPB    R0, #12
        BNE     INLOOP
        MOV     DATA, R1
        CLR     R0
        CMPB    R2, #6
        BNE     TH
        MOVB    (R1)+, R3
        SUB     #60, R3
        MUL     #1000., R3
        ADD     R3, R0
        BR      TH2
TH:     CMPB    R2, #5
        BNE     HHD
TH2:    MOVB    (R1)+, R3
        SUB     #60, R3
        MUL     #100., R3
        ADD     R3, R0
        BR      HHD1
HHD:    CMPB    R2, #4
        BNE     SMGL
HHD1:   MOVB    (R1)+, R3
        SUB     #60, R3
        MUL     #10., R3
        ADD     R3, R0
SMGL:   MOVB    (R1)+, R3
        SUB     #60, R2
        ADD     R3, R0
        RTS     PC

DATA:   .BLKW   5

DZCSR=160010
DZLPR=160012
DZTCR=160014
DZTBUF=160016
PAR1 = 12434
PAR2 = 12436
PAR3 = 12435
PAR4 = 12437
J:      .WORD   0
L:      .WORD   0
        .END    START
```

REFERENCES

1. G.H. Kinchine, and R.S. Pease, Rep. Prog. Phys. 18, 2 (1955).
2. C.W. White, J Narayan, and R.T. Young, Science 204, 461 (1979).
3. T.O. Sedgwick, J. Electrochem. Soc. 130 (2), 484 (1983).
4. C. Hill, Mat. Res. Soc. Symp. Proc. 1, 361 (1981).
5. T.E. Seidel, C.S. Pai, D.J. Lischner, D.M. Maher, R.V. Knoell, J.S. Willams, B.R. Penumalli, and D.C. Jacobson, Mat. Res. Soc. Symp. Proc. Vol.35, Materials Research Society.
6. J.C.C. Fan, R.L. Chapman, J.P. Donnelly, G.W. Turner, and C.O. Bozler, Appl. Phys. Lett. 34(11), 780 (1979), and references therein.
7. Shunji Nojima, J. Appl. Phys. 53, 5028 (1982).
8. A.H. Oraby, Y Yuba, M. Takai, K. Gamo and S. Namba, Jpn. J. Appl. Phys. 23, 326 (1984).
9. A. Chandra, Colin E.C. Wood, David W. Woodard, and Laster F. Eastman, Solid State Electronics Vol 22, 645 (1979).
10. W.E. Spicer, P.Skeath, C.Y. Sn and I. Lindau, Proc. 15th INT Conf. Physics of Semiconductors, KYOTO, 1980 J. Phys. Soc. Japan 49 (1980) Suppl. A P. 1079.
11. Edward S. Yang, Fundamentals of Semiconductor Devices (McGraw-Hill, New York, 1978), P. 124.
12. W.E. Spicer, P.W. Chye, C.M. Garner, I. Lindau, and P. Pianetta, Surf. Sci. 86, 763 (1979).
13. H. Bilz & W. Kress, Phonon Dispersion Relations in Insulators (Springer Series in Solid-State Sciences Vol 10, Springer-Vertag, New York, 1979).
14. D.E. Aspnes and A.A. Studna, Phys. Rev. B 27, 985 (1983).

15. J.F. Gibbons, W.S. Johnson, & S.W. Myloric, Projected Range Statistics Semiconductors and Related Materials (2nd ed.) (Dowden, Hutchinson, & Ross, Stroudsburg, PA, 1975).

16. B. Tell, J.E. Bjorkholm, & E.D. Beebe, Appl. Phys. Lett. 43, 655.

17. See. for example G. Abstreiter, M. Cardona, and A. Pinczuk in Light Scattering in Solids IV (Springer Topics in Applied Physics Vol. 54) (Springer, New York, 1984) P. 5; G. Abstreiter, E. Bauser, A. Fischer & K. Ploog, Appl. Phys. 16, 345 (1978); H.J. Stolz & G. Abstreiter, J. Vac. Sci. & Tech. 19, 380 (1981).

18. D. Olego & M. Cardona, Solid St. Commun. 32, 375 (1979), Phys. Rev. B 24, 7217 (1981).

19. U. Nowak, W. Richter & G. Sachs, Phys. Stat. Sol. (b) 108, 131 (1981).

20. G. Abstreiter, R. Trommer, M. Cardona, and A. Pinczuk, Solid State Commun. 30, 703 (1979), R.J. Nicholas & H.J. Stolz, Sol. St. Electron. 25, 55 (1981).

RAMAN MEASUREMENTS OF

DYE-LASER-ANNEALED, ION IMPLANTED GaAs

by

HUADE YAO

Certificate (B.S. Level), Shanghai Normal University, 1983

AN ABSTRACT OF A MASTER'S THESIS

submitted in partial fulfillment of the

requirements for the degree

MASTER OF SCIENCE

Department of Physics

KANSAS STATE UNIVERSITY

Manhattan, Kansas

1986

ABSTRACT

We have studied Raman scattering in heavily implanted, dye-laser-annealed GaAs. Samples were prepared with Sn and Cd implantations of 2, 5, and $10X10^{15}cm^{-2}$. Raman scattering was used to study the annealing behavior produced by a 10 nsec, 565 nm dye laser with a single pulse and multiple pulses. The Raman spectra indicate that the threshold for epitaxial regrowth lies between 0.2 and 0.3 J/cm^2. For Cd implantation (p-type) the carrier electrical activation appears to be very high ($\geq$50%) at low pulse energies ($\leq$0.3 J/cm^2) but decreases at high pulse energies. However, for Sn-implanted samples (n-type), best carrier activation (~ 2%) is achieved at ~ 1.6 J/cm^2 and the depletion layer width was observed to increase with the annealing pulse energy. The effects of multiple-pulse annealing of Sn-implanted GaAs at fairly low pulse energies appear to be equivalent to that of single pulse annealing at higher energies.